NASA TM X- 55 844

AN AEROSPACE NUCLEAR SAFETY
ANALYSIS OF
A Pm_2O_3 RADIOISOJET THRUSTER

JUNE 1967

GODDARD SPACE FLIGHT CENTER
GREENBELT, MARYLAND

N 67 - 32111

FACILITY FORM 602

(ACCESSION NUMBER)	(THRU)
41	/
(PAGES)	(CODE)
TMX -55844	22
(NASA CR OR TMX OR AD NUMBER)	(CATEGORY)

AN AEROSPACE NUCLEAR SAFETY ANALYSIS OF A Pm$_2$O$_3$ RADIOISOJET THRUSTER

by
William S. West
Goddard Space Flight Center
Greenbelt, Maryland

and
Andrew J. Parker, Jr. and David W. Pyatt*
Hittman Associates, Inc.
Baltimore, Maryland

June 1967

GODDARD SPACE FLIGHT CENTER
Greenbelt, Maryland

*Presently under contract to Goddard working under NAS5-10235

CONTENTS

ILLUSTRATIONS

ILLUSTRATIONS (Continued)

AN AEROSPACE NUCLEAR SAFETY ANALYSIS OF A Pm_2O_3 RADIOISOJET THRUSTER

by
Andrew J. Parker, Jr. and David W. Pyatt
Hittman Associates, Inc.
Baltimore, Maryland

and
William S. West
Goddard Space Flight Center
Greenbelt, Maryland

ABSTRACT

Interplanetary probes and earth-orbiting satellites require a propulsion capability to maintain both attitude control and to provide linear velocity increments for orbital corrections and/or interplanetary transfer trajectory corrections. Missions to Jupiter and beyond have been proposed for the 1970's to study galactic space with the ultimate aim of understanding the physics of the solar system. Small thrusters presently considered for spacecraft propulsion applications are generally classed as hot gas or cold gas-type systems. The principle of the cold gas system is to expand high pressure gas from a gas reservoir through a nozzle while the hot gas system utilizes a heat source in conjunction with a nozzle to expand the gas. This paper will deal primarily with the application of a nuclear heat source and its suitability to meet reasonable aerospace nuclear safety criteria when incorporated into a pulse jet thruster design.

AN AEROSPACE NUCLEAR SAFETY ANALYSIS OF A Pm_2O_3 RADIOISOJET THRUSTER

INTRODUCTION

The nuclear thruster, which will be used as the basis of the safety analysis for this paper, is known as the Radioisojet (RIJ). An RIJ design concept was investigated under a joint NASA-Goddard/AEC R and D program with the General Electric Company, Cincinnati, Ohio and Battelle Northwest, Richland, Washington, as the major contractors. Feasibility of RIJ low thrust level nuclear thrusters was demonstrated by a successful ground hot-firing test program conducted at Mound Laboratory, Miamisburg, Ohio in late 1966 where expected propulsion capabilities were achieved. A schematic of this thruster is presented in Figure 1.

In conjunction with the test program, Hittman Associates, Inc. performed a preliminary nuclear safety study of the RIJ for NASA-Goddard due to the toxic and radiological health hazards of the nuclear source (Pm_2O_3) and to develop a safety analysis methodology early in the RIJ development program. The thruster that is analyzed in this paper was not designed as, or intended to be, flight hardware and therefore aerospace nuclear safety was not a hardware design consideration. The analysis techniques developed during this study are presented by this paper. The atmospheric reentry analysis is unique in that it considers the oxidation and ablation of refractory metals. (To date, virtually no analyses have been performed on the aerothermal oxidation of refractory metals other than tantalum. A refractory metal was selected for the capsule liner for the following reasons: the high temperature at which the capsule operates, the increased protection it offers under reentry conditions, and the good structural qualities at high temperatures indicated for these materials.)

It was assumed that the missions to which the RIJ would be assigned would require either a parking orbit (near earth) or would be direct launch, deep space probes. A decision was made to examine the parking orbit situation for the study as the energy levels experienced by the RIJ from a parking orbit decay would present a worst case nuclear safety hazard. A scoping analysis was performed to define the RIJ launch vehicle, mission type, and abort environment. Based upon the results of the scoping analysis, a detailed analysis was performed to evaluate the potential of the radioisojet fuel capsule to reenter the earth's atmosphere and/or burn up and will be presented in this paper.

1

TECHNICAL DISCUSSION

A. Basic Aerospace Nuclear Safety Criteria

A single safety criterion can be stated: that no undue hazard to people or property be caused by a foreseeable normal or unusual result of the launch. However, this is not very definitive, and certain more specific design criteria (a form of development target) are necessary. In virtually all isotope space system designs, one of the most difficult problems is safe return and ultimate disposal of the fuel. The fuel must be safely contained in the event of a launch pad fire, a return to earth on launch abort, a short-lived orbit, or, finally, if a successful mission occurs, after many years in high temperature operation.

Past radioisotope space systems and those under present development have been designed using the following general guidelines for aerospace nuclear safety.

1. Launch

a. During launch and ascent, the fuel capsule must completely contain the nuclear fuel under all abort environments to which it would be exposed.

b. For launch aborts which may yield trajectories where partial burn-up and impact of an unclad fuel mass occurs, the rocket trajectory must be such that impact takes place in a remote unpopulated area.

2. Reentry

a. During reentry, the fuel capsule must completely burn up under the action of aerodynamic heating and the fuel be reduced to below $1\,\mu$ in average debris size above 100,000 feet. The latter condition assures an adequately low ultimate ground hazard from the ensuing fallout.

b. Complete containment under reentry and impact/burial conditions may be chosen for fuels of short half life and low direct radiation hazard or when the fuel inventories are so large that release to the atmosphere is intolerable.

3. Inert Fuel Forms

An intermediate safety philosophy applicable to inert fuels also exists; that of the microsphere fuel form. The basic safety philosophy here

explores the middle ground between complete containment and burnup. It allows the containment to be breached during reentry and releases the fuel form which is in a stable high temperature microsphere form. The individual microspheres then decelerate rapidly and survive reentry. (This philosophy is not applicable to the RIJ Pm_2O_3 fuel capsule as it is not in an inert fuel form.)

Based upon the character of the radioisojet fuel form chosen for the RIJ design, Pm_2O_3, it would seem that the criterion of complete burnup above 100,000 feet would be impossible to achieve at parking orbit decay or launch vehicle abort reentry velocities. The heat capacity, melt temperature and high emissivity of the fuel form is such that total fuel burnup is not expected. This point is investigated in depth in Section C. and is confirmed. Therefore intact reentry of the radioisojet must be the criterion on which the design should be based.

B. The Radioisojet Abort Environment

Figure 2 presents a portion of a typical "Abort Events and Probabilities" chart for an aerospace nuclear satellite system. (This chart is typical of a space probe which may use a radioisotope generator.) The portion of the diagram which is presented represents the system logic from an altitude in the ascent trajectory of approximately 500,000 feet to spacecraft injection into its desired orbit. Based on this logic diagram, it can be seen from the asterisked steps that the key safety consideration areas fall into the category of random reentry from a short lived orbit.

The Thorad Agena D was selected as the typical launch vehicle suitable to be used for radioisojet missions. This vehicle is being used for the NASA Goddard Nimbus B/SNAP-19 program, and the experience gained, particularly in the area of nuclear safety, will be applicable to the radioisojet analysis. (It is felt that the variation of launch parameters for other boosters will not change sufficiently to alter the major results of this paper.)

Aborts on the pad and during the initial stages of lift-off which yield impact in the launch area can be quickly brought under control. Aborts along the pre-orbital trajectory will yield deep water impact and burial.

Aborts late in the ascent phase which reduce final injection velocity or angle present the greatest problem. They will result in failure to achieve full orbit or will produce an elliptical orbit with low apogee. The atmospheric drag at the apogee will quickly degrade the orbit, and under these circumstances reentry becomes a random event with a high probability of land impact. Prediction of

the location of impact points on the earth's surface is quite difficult and recovery of the fuel source becomes improbable; hence this situation causes the greatest potential hazard.

Based upon the foregoing discussion, the following reentry parameters shown in Table I shall be used in Section C. to determine the survival potential of the radioisojet fuel capsule.

Table I.
Reentry Parameters

Reentry Mode	Altitude (ft.)	Flight Angle (deg.)	Velocity (ft/sec)
Parking Orbit Decay Attached to Spacecraft	400,000	-0.1°	25,600
Parking Orbit Decay Released at 280,000 ft	280,000	-1.12°	25,200
Abort at EVM* Released	536,740	-0.037°	18,239
Abort at EVM Attached to Spacecraft	536,740	-0.037°	18,239

*EVM (Enable Velocity Meter)—Transfer Ground Control to Agena

C. Evaluation Analysis

1. Introduction — Based upon the arguments presented in Section B., a reentry burnup analysis was performed on the radioisojet thruster for a parking orbit decay trajectory and for an abort occurring along the booster ascent curve at EVM. Release modes of the thruster are an important consideration and are very difficult to estimate. Hence the definition of the envelope of all possible reentry destruction cases was derived by assuming both thruster release from any spacecraft at 280,000 feet and attached to a tumbling hypothetical spacecraft. For abort at EVM, it is assumed that the thruster can be either released at the start of abort or remain attached to the same hypothetical spacecraft. The spacecraft chosen was a cylinder, 3 feet in diameter and 4 feet long, weighing 1100 pounds. Selection of the hypothetical spacecraft was arbitrary; however, it was felt that for this analysis any reasonable satellite in the 1000-1500 pound

range was adequate. The one selected was chosen to demonstrate how the burn-up calculations can be made for any known spacecraft ballistic coefficient and nose radius.

The cases of the radioisojet thruster release at 280,000 feet for the parking orbit decay trajectory and at the start of abort for the abort trajectory, while not being compatible with the present design, were selected because the thruster and capsule would receive the maximum aerodynamic heating. For these cases the spacecraft would not shield the assembly from the free stream flow. Further, the ballistic coefficient for the thruster is larger than a typical spacecraft ballistic coefficient, and the thruster nose radius is an order of magnitude smaller than that for a spacecraft. These effects increase the aerodynamic heating to the released thruster configuration.

The thermal model selected to calculate heat transfer by conduction through various zones of the thruster assembly during reentry was a one-dimensional section through the capsule and inner and outer liners minus the Nichrome V insulation. A one-dimensional analysis was considered sufficient to give approximate heat transfer rates in the radial direction, and the end effects of the capsule were considered to be negligible.

2. Reentry Trajectory Calculations — The equations of motion in a two-dimensional plane were solved to calculate the altitude, velocity and flight angle versus time for the parking orbit decay and four booster abort trajectories. It should be noted that the variation of altitude and time between a released and attached thruster for the four abort trajectories studied was less than 1 percent. Figure 3 presents the parking orbit decay reentry for the attached and released thruster. Also shown are the altitude where the refractory inner liner is first exposed and where this liner is completely oxidized. Altitude versus time curves for four abort trajectories are shown in Figure 4 and in Figure 5 for the abort occurring at EVM. Table II lists the primary events along the Thorad-Agena D launch ascent which can lead to a mission abort.

The equations of motion of a reentering object as derived by Chapman[1] are listed below. A spherical earth and atmosphere as well as a non-rotating earth were assumed.

$$- \frac{d^2 y}{dt_2} = \frac{dv}{dt} - g - \frac{u^2}{r} - \frac{L}{m} \cos \Phi + \frac{D}{m} \sin \Phi \qquad (1)$$

$$\frac{du}{dt} + \frac{uv}{r} = \frac{-D}{m} \left(\cos \Phi + \frac{L}{D} \sin \Phi \right); \quad \tan \Phi = v/u \qquad (2)$$

TABLE II
Primary Events along Nominal Ascent Trajectory which can lead to Mission Abort

Event	Time From Liftoff (sec)	Description	Abort Point Range (N.M.)	Abort Velocity (ft/sec)	Instantaneous Impact Point		
					Range (N.M.)	Latitude (Deg.)	Longitude (Deg.)
SBB	40.00	Solid Booster Burnout	0.84	1,050.3	4.136	34.68	120.64
EBM*	98.00	Eject Booster Motors	8.15	2,059.6	40.64	34.09	120.82
	124.00	Initiate WECO Guidance	19.45	3,459.0	96.29	33.20	121.11
MECO*	218.33	Thor Main Engine Cutoff	121.68	13,163.3	820.67	21.47	124.51
VECO*	227.33	Thor Vernier Engine Cutoff	140.57	13,156.5	826.93	21.37	124.53
SEP*	232.33	Separation of Agena/Thor	150.96	13,124.0	826.93	21.37	124.53
4	245.33	Start Fast Pitch	179.23	13,042.4	826.97	21.37	124.53
5*	252.33	Agena Ignition	190.53	13,012.6	826.98	21.37	124.53
6	253.83	Full Agena Guidance In Operation	195.81	13,010.1	827.84	21.37	124.53
7*	262.33	Fire Nose Shroud Squibs	220.2	13,326.8	857.1	21.00	124.6
EVM	386.20	Transfer Ground Control to Agena	519.83	18,239.5	1,298.8	13.68	126.5
8	409.33	Shutdown WECO System	602.4	19,903.2	1,493.8	10.51	127.2
AECO	485.95	Agena First Burn Cutoff	870.1	26,788.2	—	—	—

* Primary Event

A sketch of a reentering object is shown in Figure 6 where:

$$D = \frac{1}{2} C_D \rho A V^2 = \text{total drag}$$

$$L = \frac{1}{2} C_L \rho A V^2 = \text{total lift}$$

$$V = \sqrt{u^2 + v^2} = \text{resultant velocity}$$

The magnitude of the resultant force is:

$$F = \left[(-mg + L \cos \Phi - D \sin \Phi)^2 + (D \cos \Phi + L \sin \Phi)^2 \right]^{0.5} \qquad (3)$$

where:

A = reference area for drag and lift, square feet

C_D = drag coefficient

C_L = lift coefficient

D = drag force, pounds

g = gravitational acceleration, ft/sec^2

L = lift force, pounds

m = mass of vehicle, slugs

r = distance from planet center, ft

t = time, seconds

u = circumferential velocity component normal to radius vector, ft/sec

y = altitude, ft

v = vertical velocity component (along direction of radius vector), ft/sec

V = resultant velocity, ft/sec

Φ = flight path angle relative to local horizontal direction, negative for descent, degrees

Equations (1) through (3) are solved using the Runge-Kutta finite difference technique starting at a specified initial reentry point.

The hypersonic drag coefficients for the various partially burned thruster configurations are listed in Table III below.

Table III
Hypersonic Drag Coefficients

Configuration	C_D
1. End-over-end tumbling* fuel capsule [2]	0.727
2. End-on stable fuel* capsule [2]	0.489
3. End-on stable thruster minus outer shell and [3] radiation insulation	2.165
4. End-over-end tumbling* cylindrical spacecraft [2]	0.936

*Reference area = LD

Since the radiation insulation is burned away early in the aerodynamic heating regime, the drag coefficient of the thruster minus the insulation was used in the trajectory calculations until the stainless steel flange ablated.

3. Aerodynamic Heating — Aerodynamic heating will only be considered for laminar, continuum hypersonic flow and for hypersonic free molecular flow. The effect of "blocking" due to vapor injection into the boundary layer flow will not be considered as the materials of the thruster have relatively low vapor pressures at the reentry temperatures, and hence are expected to melt well before appreciable vaporization takes place.

The equation [2] describing the stagnation point heating rate to a coldwall catalytic sphere in hypersonic continuum flow is:

$$\dot{q}_s = \frac{17,600}{\sqrt{r}} \left(\frac{\rho}{\rho_{S.L.}}\right)^{0.5} \left(\frac{V}{V_c}\right)^{3.15} \left(\frac{BTU}{ft^2\text{-sec}}\right) \quad (4)$$

$\rho_{S.L.}$ = air density at sea level

V_c = circular orbital velocity — 25,600 ft/sec at 400,000 feet

r = effective nose radius, feet

ρ = density

For free molecular flow, the heating rate to a flat plate perpendicular to the flow is given as [4] :

$$\dot{q} = aH_o \left(\rho_\infty V_\infty\right) \quad (5)$$

$$\dot{q} = \frac{a \rho_\infty V_\infty^3}{1556} \quad \frac{BTU}{ft^2\text{-sec}} \quad (6)$$

a = accommodation coefficient = $\dfrac{E_i - E_r}{E_i - E_w}$, where

E_i = energy brought to the wall by indicent molecules

E_r = energy carried away by reemitted molecules

E_w = energy that would be carried away if the reemitted air were at wall temperature

H_o = stagnation enthalpy

In reality there are at least 6 different flow regimes between continuum flow and free molecular flow. However, the present analysis will assume a transition from free molecular flow to continuum flow at a Knudsen No. $\left(\frac{\lambda}{D}\right)$ of 1. Cropp [2] presents data for merging the transition flow between continuum and free molecular flow by using the non-dimensional Stanton No. $\left(\frac{Nu_2}{Pr_2 \, Re_2}\right)$, and

a more refined analysis would include this transition zone into the aerodynamic heating code.

Equation (4) above for stagnation point heating to a sphere must be modified to find the average heating rate (Fq) in the continuum flow regime for the cylindrical configuration.

$$Fq = \frac{local\ heating\ rate}{stagnation\ heating\ to\ a\ sphere\ of\ same\ radius}$$

Klett [4] has derived expressions for the continuum ratios for cylinders and spheres. The values used to calculate the aerodynamic heating rates for the radioisojet are listed in Table IV below.

Table IV
Average Continuum Flow Heating Rate Surface Averaging Factors

Configuration	F_q
1. End-over-end tumbling cylinder-end	0.329
2. End-over-end tumbling cylinder-sides	0.178 (L/D=3)
3. End-on-stable flat plate (flange)	0.613
4. End-on-stable cylinder – end	0.613
5. End-on-stable cylinder – side	0.088
6. End-over-end tumbling cylinder (spacecraft) – end	0.329
7. End-over-end tumbling cylinder (spacecraft) – side	0.194 (L/D=1.33)

The heating rate versus time curves are calculated using a Hittman Associates, Inc. aero computer code which solves the trajectory equations in the previous section and calculates the heating rate from the known velocity and density.

Aerodynamic heating rates versus time for the parking orbit trajectory and abort at EVM trajectory are shown in Figures 7 through 10 for both the attached and released modes.

4. **Reentry Burnup Thermal Model** — The credibility of the results of an ablation or burnup analysis is largely determined by the accuracy and arrangement of a proper thermal model. There is no set of rules or equations by which the engineer can create the proper number of nodes and the proper arrangement. Thermal modeling becomes an art, and only experience coupled with good judgment yield proper results. For this analysis, a one-dimensional model, taking a cut through the fuel and capsule, was used for the thruster heat transfer analysis. It is considered that, while the relatively massive ends of the capsule will act as a heat sink, the one-dimensional model will predict with fair accuracy the radial conduction heat transfer. A sketch of the thermal model is shown in Figure 11.

The unsteady state heat transfer equation to evaluate conduction and radiation heat transfer is solved by the finite differences technique. The TAP-3 digital computer code (Hittman Associates, Inc. Thermal Analyzer Program) utilizes the forward difference scheme to solve the finite difference equations.

The heat transfer differential equation can be written in finite differences as:

$$T_{i,\theta+\Delta\theta} = T_{i,\theta} + \frac{\Delta\theta}{C_i} \left[Q_i + \sum_j Y_{i,j} T_{j,\theta} - T_{i,\theta} \sum_j Y_{i,j} \right] \qquad (7)$$

where:

θ = time

T = temperature

Y = admittance or conductance between nodes

i = subscript referring to node being considered

j = subscript referring to nodes connected to node i

Q = internal or external heat added to a node

C = total capacitance of a node

For radiation from node i to node j, the equation is:

$$Y_{i,j} = \sigma A_i F_{i,j} \epsilon_i \epsilon_j \left(T_i^2 + T_j^2\right)(T_i + T_j) \tag{8}$$

σ = Stephan Boltzmann constant

A_i = area of node i

$F_{i,j}$ = view factor from node i to j

ϵ = total hemispherical emissivity for gray body radiation

Any set of units can be used with Equation (7) as long as they remain consistent. For purposes of this analysis the units chosen were BTU, inches, degrees F, and seconds.

A preliminary survey of the properties of typical capsule liner materials indicates that they have a high oxidation potential above 500°F. It was felt since the capsule liner was exposed to the free stream flow at a temperature of approximately 2200°F that oxidation would immediately begin and that the liner would oxidize before it achieved its melt temperature. (This is discussed in Section 5.)

The temperature history for the thermal model is shown in Figures 12 and 13 for the parking orbit decay trajectory and in Figures 14 and 15 for the EVM abort trajectory.

The various sequences of reentry burnup for the released thruster are shown in Figure 16 schematically and in Figure 17 for both the attached and released modes.

5.   Oxidation of Refractory Liner Under Reentry Conditions — The high melt temperature associated with typical refractory metals (approximately 3300°F minimum) coupled with the relatively high oxidation potential at moderately high temperatures indicates a good probability that, under aerothermal reentry conditions, they will oxidize before melting. This assumption has been born out by the analysis performed for the RIJ. A literature search yielded limited results for the oxidation of refractory metals under reentry conditions. However, Sandia Corporation has performed tests in a hypothermal plasma tunnel on the oxidation of tantalum under simulated reentry conditions. An analytical study was made to correct the empirical oxidation rate equations for

12

tantalum to similar conditions for a general refractory material. It must be noted that in the following analysis, the derivation of the theoretical equations by Marshall[5] is somewhat nebulous, and the resulting equations must be used with caution. However, the data trends are expected to be valid, although the magnitude of the oxidation rate may not be exact.

Marshall[5] of Sandia Corporation has derived an expression for the rate of recession of a tantalum surface under analogous conditions. His assumptions include:

(a) The reacted material is continuously removed from the surface to further expose bare metal.

(b) All the oxygen that diffuses to the surface is reacted.

The validity of these assumptions when applied to another refractory metal was considered. (The validity of the second assumption was experimentally demonstrated for tantalum[5].) It is probable that at the relatively low oxygen fluxes available in the upper atmosphere, assumption (b) holds for those metals where assumption (a) is correct. It, therefore, appears reasonable to accept Marshall's assumptions for a refractory subjected to a free stream temperature in excess of approximately 2000°F.

The equation derived by Marshall and closely confirmed by experimental results consists of a product of two terms, one of which involves the rate of availability of oxygen at the surface, and the second involves the quantity of metal removed per quantity of oxygen reacting. It is this latter term which must be adjusted to convert the expression from tantalum to some other refractory metal.

For the general reaction of any metal (Me)

$$x \, Me + y/2 \, O_2 \longrightarrow Me_x O_y \tag{9}$$
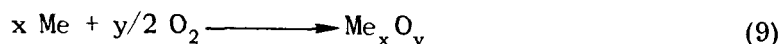
the rate of metal removal (inches/sec)

$$\frac{\Delta L}{\Delta \theta} = \left(\frac{2x}{y}\right) \left(\frac{At \ Wt \ of \ the \ Metal}{Density \ of \ the \ Metal}\right) \left(\frac{Surface \ Oxygen \ Flux}{Mol \ Wt \ of \ O_2}\right) \tag{10}$$

$$\frac{\Delta L}{\Delta \theta} = oxidation \ rate$$

For tantalum, excellent correlation was achieved between analytical and experimental results when the oxide composition "TaO" was assumed. Although no such oxide exists, a eutectic between Ta and Ta_2O_5 at approximately the "TaO" composition has been reported, and experimental studies indicate that the product removed from the tantalum surface is indeed a mixture of Ta_2O_5 and tantalum metal.

Under these conditions the equation derived by Marshall becomes

$$\frac{\Delta L}{\Delta \theta} = 0.00545 \, \Delta X_o \left[\frac{P_{t2}}{R_e} \right]^{1/2} \tag{11}$$

where: ΔX_o = mass fraction of oxygen in the gas

P_{t2} = total pressure behind the normal shock wave in lb/ft^2

R_e = effective nose radius in feet

To convert Equation (11) from tantalum to a second material, one must solve for the term

$$\left(\frac{2x}{y} \right) \left(\frac{At \ Wt \ of \ the \ Metal}{Density \ of \ the \ Metal} \right)$$

for both the material of choice and tantalum. The ratio of these two values is multiplied into the constant of Equation (11).

For tantalum if the reaction is assumed to be

$$Ta + 1/2 \ O_2 \longrightarrow TaO$$
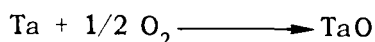
then

$$\left(\frac{2x}{y} \right) \left(\frac{at \ Wt. \ of \ Ta}{Density \ of \ Ta} \right) = \frac{2(180.948)}{1037} = 0.348$$

For the refractory metal of interest, one must define the following limits:

(a) The most stable oxide – $Me_{xs} O_{ys}$

(b) The case in which rate of metal removal is the greatest – $Me_{xg} O_{yg}$ (where subscript s refers to stable and g refers to greatest).
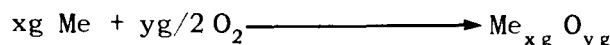
14

If the reaction is

$$xs\ Me\ +\ ys/2O_2 \longrightarrow Me_{xs}O_{ys}$$
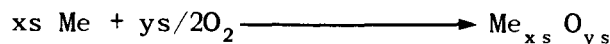
then

$$\left(\frac{2x}{y}\right)\left(\frac{at\ Wt.\ of\ Me}{Density\ of\ Me}\right) = \left(\frac{2\ xs}{ys}\right)\left(\frac{W_{Me}}{\rho_{Me}}\right) = S$$

and if the reaction is

$$xg\ Me\ +\ yg/2\ O_2 \longrightarrow Me_{xg}O_{yg}$$

then

$$\left(\frac{2x}{y}\right)\left(\frac{at\ Wt.\ of\ Me}{Density\ of\ Me}\right) = \left(\frac{2\ xg}{yg}\right)\left(\frac{W_{Me}}{\rho_{Me}}\right) = G$$

Therefore, if the reaction product is $Me_{xs}O_{ys}$, Equation (11) becomes

$$\frac{\Delta L}{\Delta \theta} = (0.00545)\left(\frac{S}{0.348}\right)\Delta X_0 \left[\frac{P_{t_2}}{R_e}\right]^{1/2} \tag{12}$$

and if $Me_{xg}O_{yg}$ is the reaction produce, the equation becomes

$$\frac{\Delta L}{\Delta \theta} = (0.00545)\left(\frac{G}{0.348}\right)\Delta X_0 \left[\frac{P_{t_2}}{R_e}\right]^{1/2} \tag{13}$$

Equations (12) and (13) represent the probably lower and upper limits for the recession rate of the surface considered under reentry conditions. The reader is cautioned that it has not been possible to derive Marshall's equation, and until its validity is determined care must be exercised in applying the results of this analysis. Equations (12) and (13) were used to determine the RIJ's potential to survive under reentry heating conditions.

6. <u>Burnup and Impact Zones</u> — The booster launch trajectory and the trajectory for partial burnup for both modes of thruster reentry are shown in Figure 18. Partial burnup is defined, for this case, as thermal destruction of the thruster and fuel capsule liners. It can be seen that a booster abort before 350 seconds will allow the thruster to reenter and land without exposing the fuel slug. It was determined that for a booster abort after 350 seconds the fuel slug will be exposed by the action of reentry heating and will reach the ground intact and partially encapsulated.

Terminal velocity versus altitude for the intact thruster and partially burned capsule configurations is shown in Figure 19. Figure 19 is the envelope of impact velocity for the possible intact and partially burned configurations.

Further investigation has shown that redesign of the radioisojet to achieve complete intact reentry appears to be possible without affecting the design function or efficiency of the RIJ. This redesign involves repositioning of certain key RIJ components such as fuel lines and mounting flange as well as adding a reentry heat shield. A general increase of the system weight will result and is estimated to be from 40 percent to 60 percent of the present RIJ weight. This appears to represent a slight weight change to the total spacecraft systems of which the RIJ will be a part to achieve the necessary safety confidence level.

CONCLUSIONS

Based on the analysis presented in this paper the following conclusions were reached:

(1) Analysis techniques (methodology, mathematical model, and appropriate computer logic) developed for previous space applications can be applied early in a nuclear R and D space program, to evaluate an aerospace component or system and determine its safety potential.

(2) It is desirable in the development of a new device which incorporates a nuclear source to initiate nuclear safety studies as early in the program as possible. These studies must be performed prior to beginning the flight hardware development phase of a program in order that modifications can be easily integrated into the design. It is impossible to optimize a component or system without the knowledge of design criteria similar to these generated in this paper. Specific application of these criteria to the RIJ indicate that:

(a) There are several reentry/abort situations which neither permit the fuel capsule in the current thruster design to reenter intact not the fuel slug to burn up and disperse in the upper atmosphere (above 100,000 feet). See Figure 18.

(b) Complete intact reentry of the RIJ appears to be possible by the addition of a reentry heat shield without appreciably affecting the design function or efficiency.

REFERENCES

1. Chapman, Dean R. - "An Approximate Analytical Method for Studying Entry into Planetary Atmospheres," NACA TN 4276, 1958.

2. Cropp, L. O. - "Analytical Methods Used in Predicting the Reentry Ablation of Spherical and Cylindrical Bodies," Sandia Corporation Report, SC-RR-65-187, 1965.

3. Hoerner, S. F. - Fluid Dynamic Drag, Self Published, 1965.

4. Klett, Robert D. - "Drag Coefficients and Heating Ratios for Right Circular Cylinders in Free-Molecular and Continuum Flow From Mach 10 to 30," Sandia Corporation Report, SC-RR-64-2141, 1964.

5. Marshall, B. W. - "An Experimental Study of the Effect of Oxygen on Tantalum Ablation in a Hyperthermal Plasma Tunnel," Sandia Corporation Report, SC-RR-65-615, 1966.

NH₃ INLET

GAS FLOW
CHANNEL

THERMOCOUPLE

STAINLESS STEEL
SUPPORT
FLANGE

NICHROME
HEAT SHIELD

Pm_2O_3 FUEL

H_x

H_x

NOZZLE

DOUBLE CLADDING
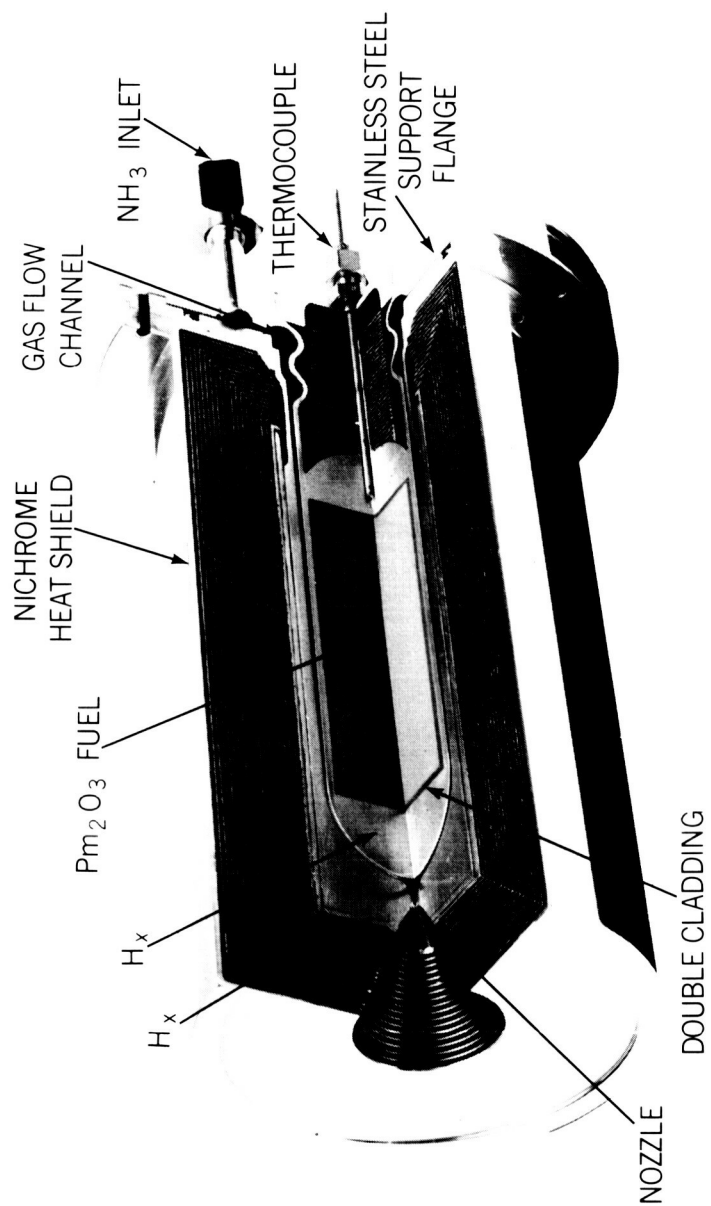
Figure 1. Radioisojet Schematic

PORTION OF A TYPICAL

AEROSPACE SAFETY LOGIC CHART - ABORT EVENTS AND PROBABILITIES
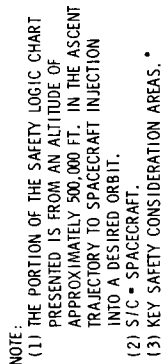
Figure 2. Typical Aerospace Safety Logic Chart
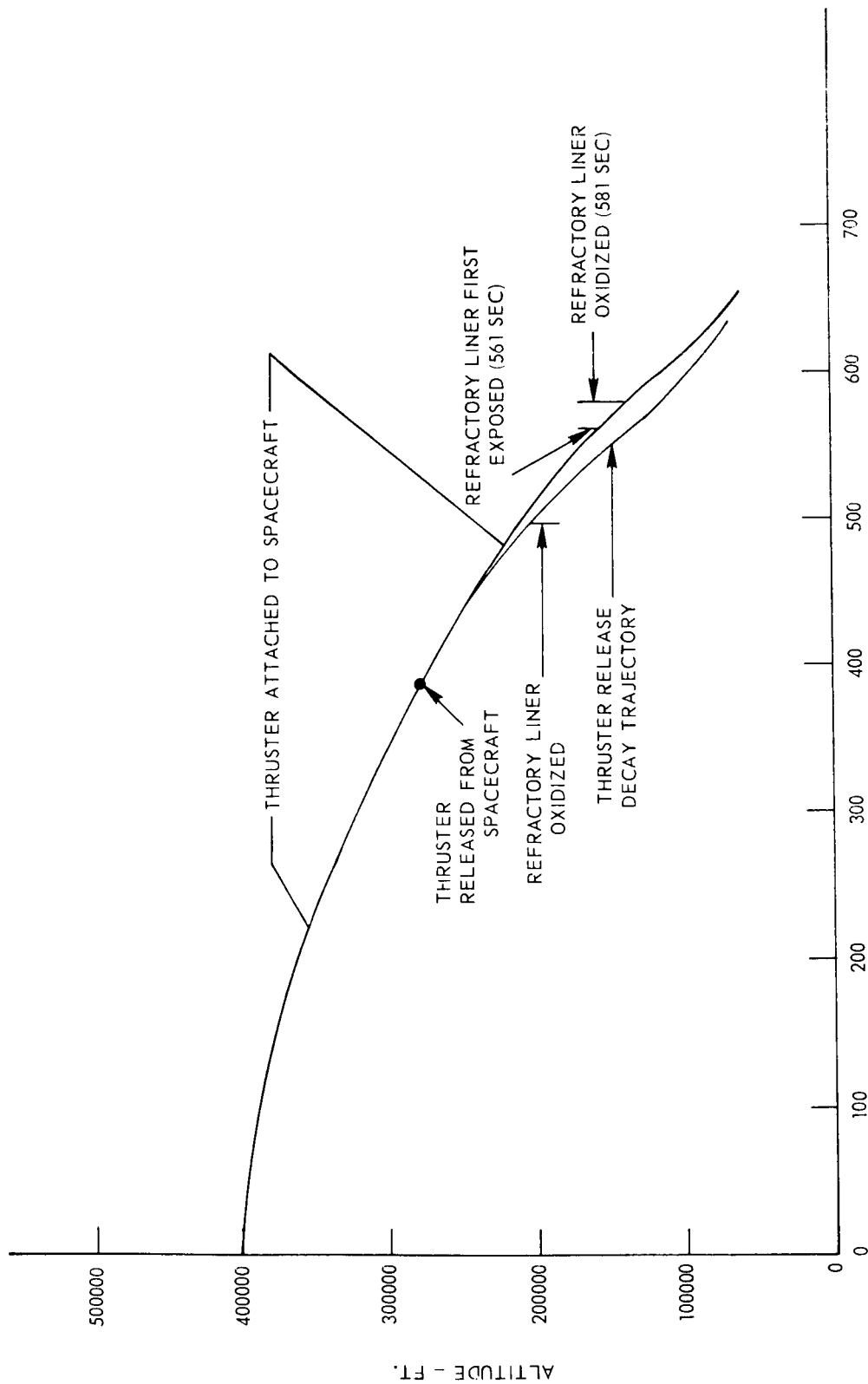
Figure 3. Radioisojet Altitude vs Time-Parking Orbit Decay Reentry

ALTITUDE - FT × 10.³

TIME FROM START ABORT - SEC.

MECO (MAIN ENGINE CUT OFF)

SEPARATION

262.33 SEC

EVM

NOTE – CURVES SHOWN FOR
RELEASED THRUSTER – SPACECRAFT
TRAJECTORY VARIED APPROX. 1%
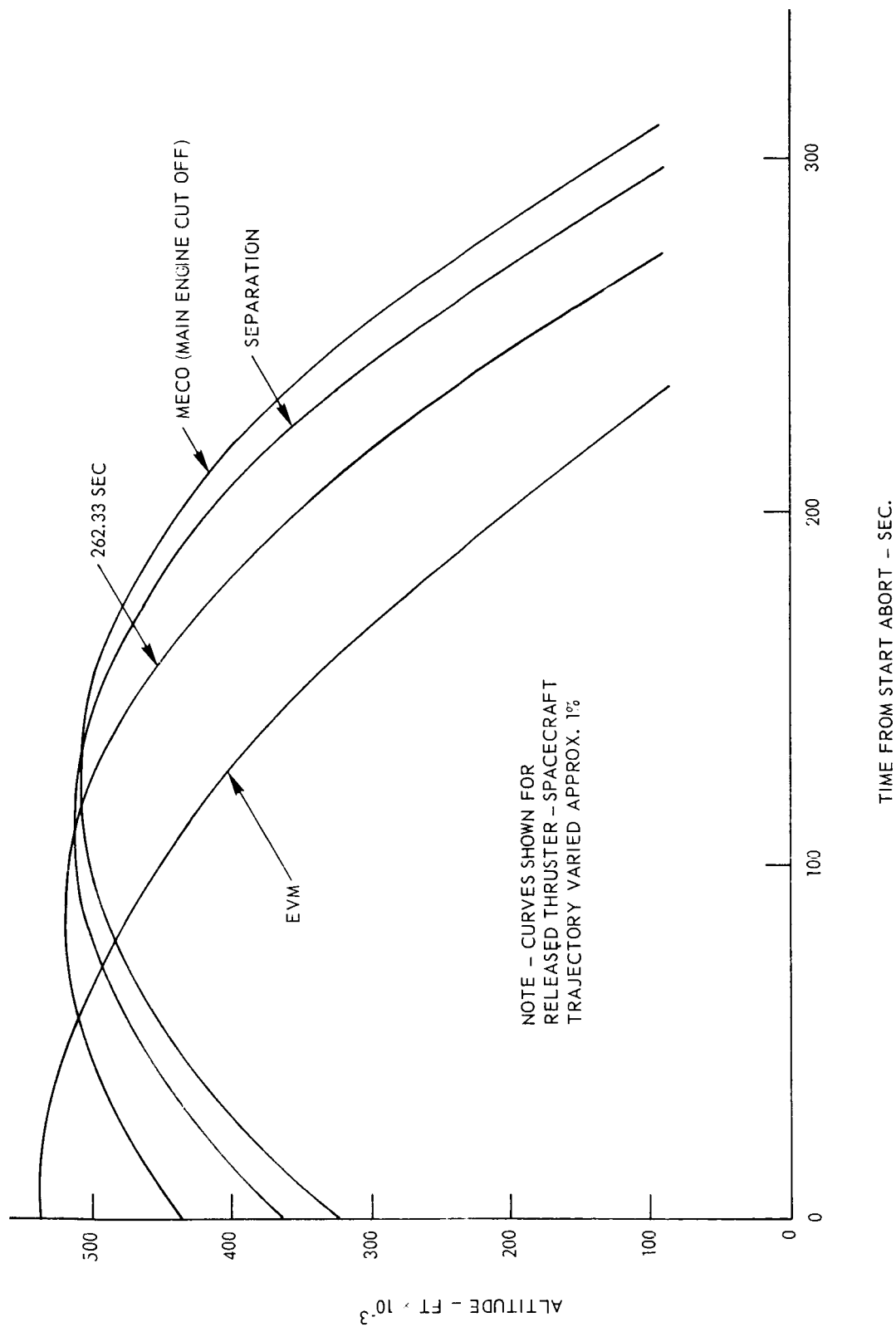
Figure 4. Radioisojet Reentry Altitude vs Time For Various Booster Aborts

21
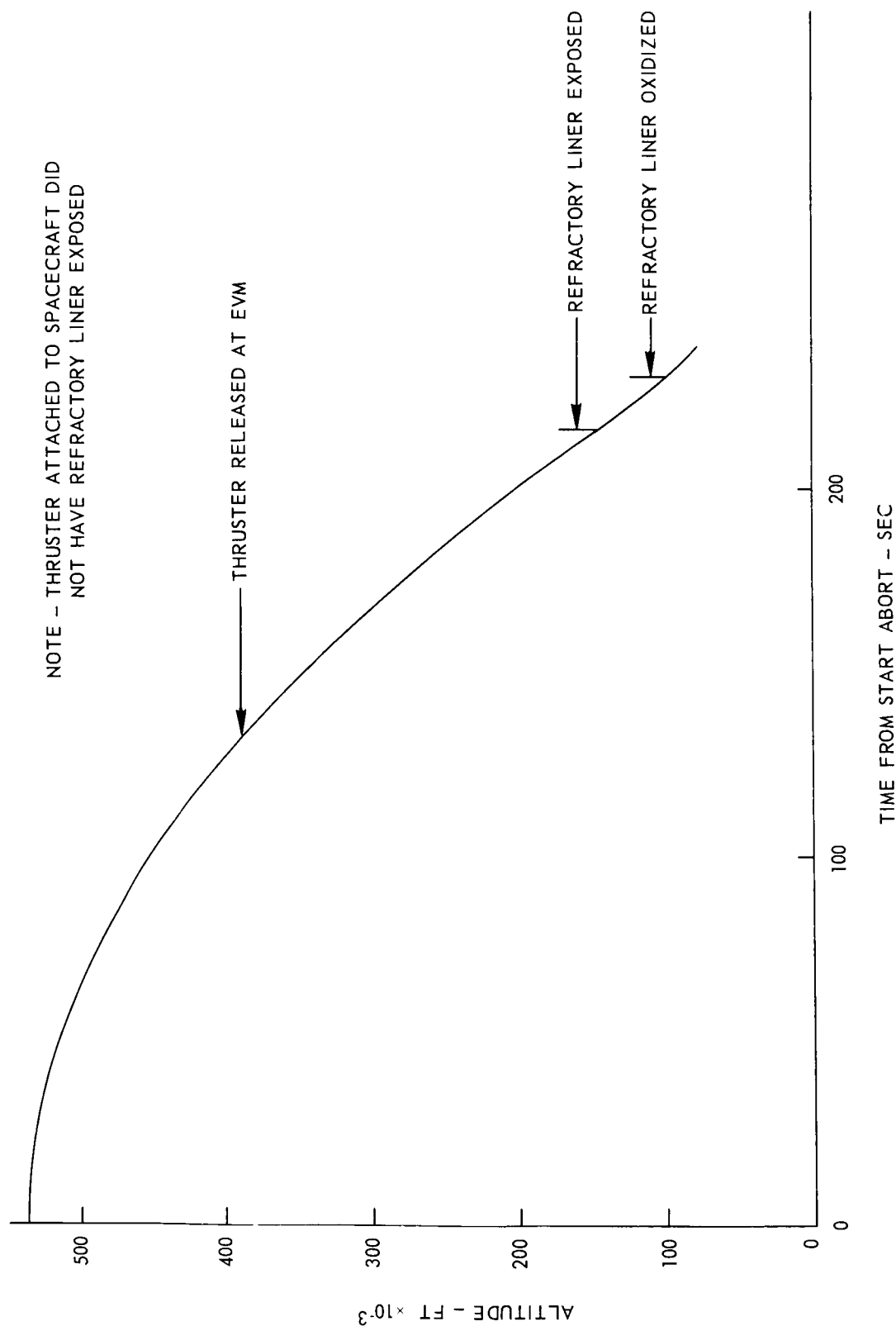
Figure 5. Radioisojet Altitude vs Time-Booster Abort At EVM Attached To Spacecraft

22
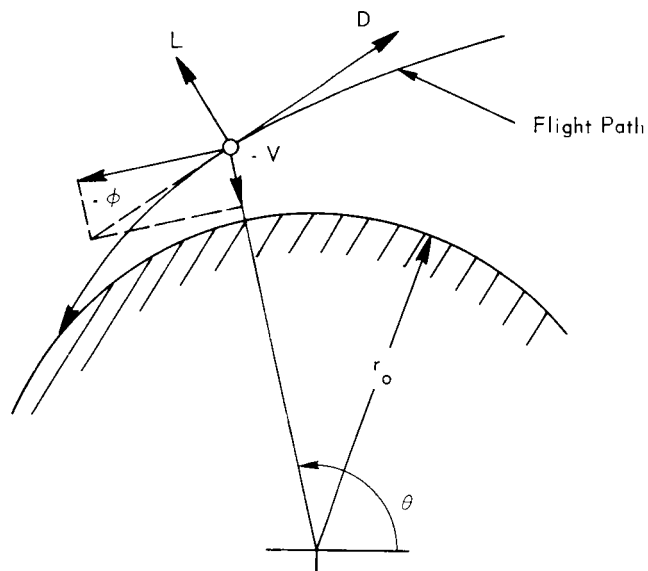
Figure 6. Force, Velocity Diagram
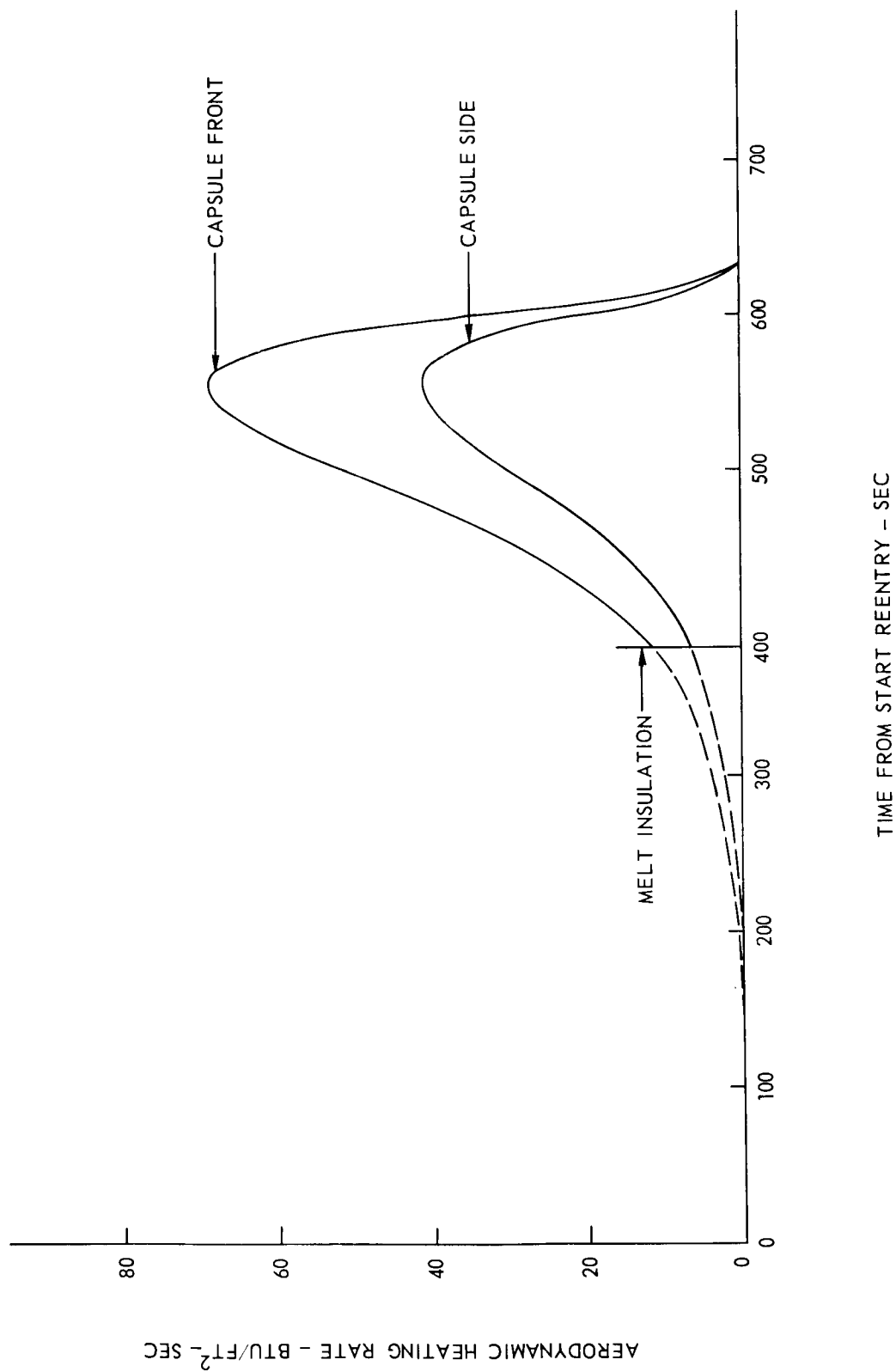
Figure 7. Radioisojet Thruster Attached To Tumbling Spacecraft Parking Orbit Decay Trajectory Aerodynamic Heating

24
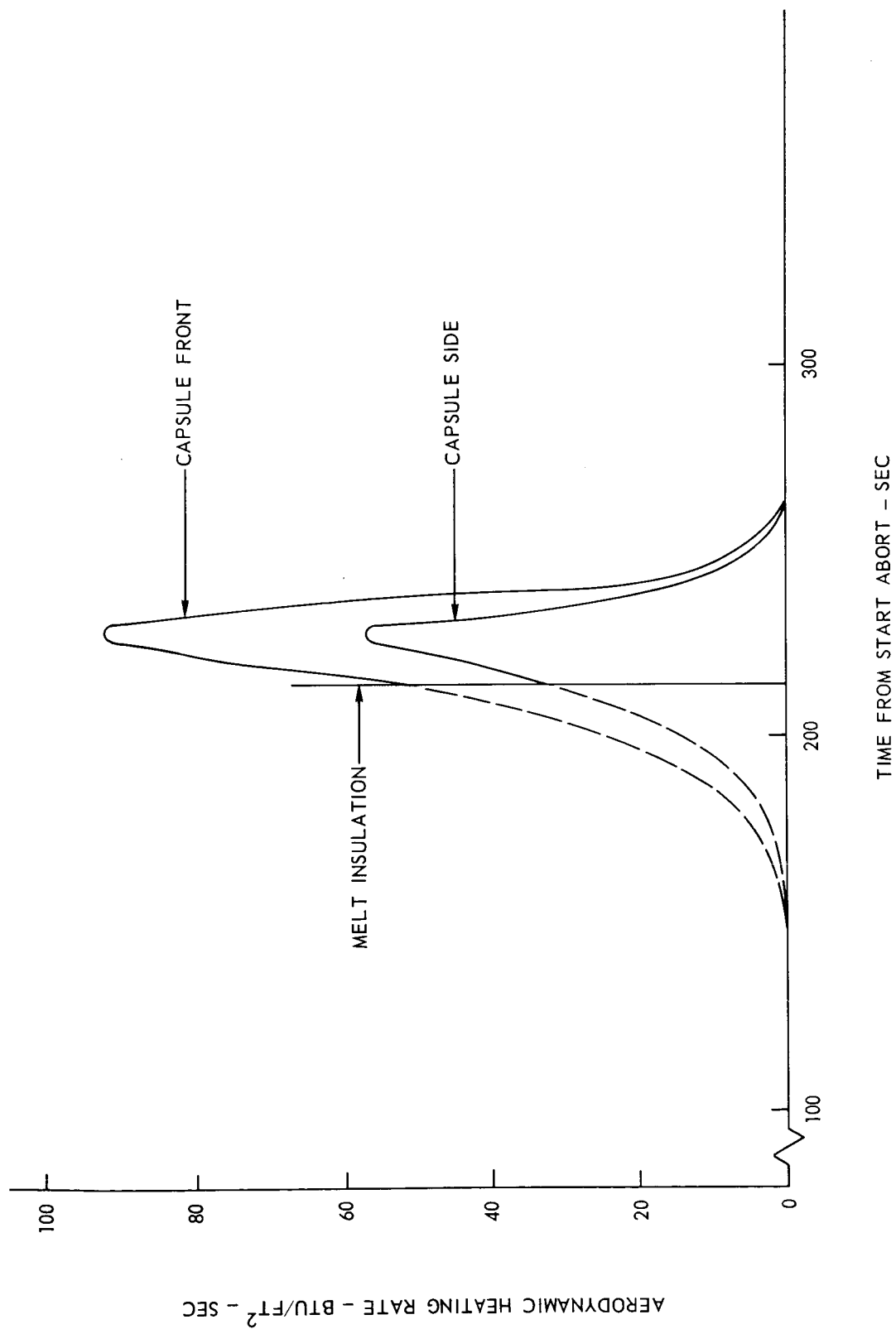
Figure 8. Radioisojet Thruster Attached To Tumbling Spacecraft Booster Abort At EVM Aerodynamic Heating

25

AERODYNAMIC HEATING RATE – BTU FT^2 – SEC

TIME FROM 280,000 ft – SEC

FLANGE – END ON STABLE

FRONT THRUSTER ASSEMBLY
TUMBLING

SIDE TUMBLING CAPSULE
AFTER FLANGE ABLATES

SIDE TUMBLING
ASSEMBLY

SIDE – END ON STABLE

FLANGE
ABLATE

INSULATION
MELT
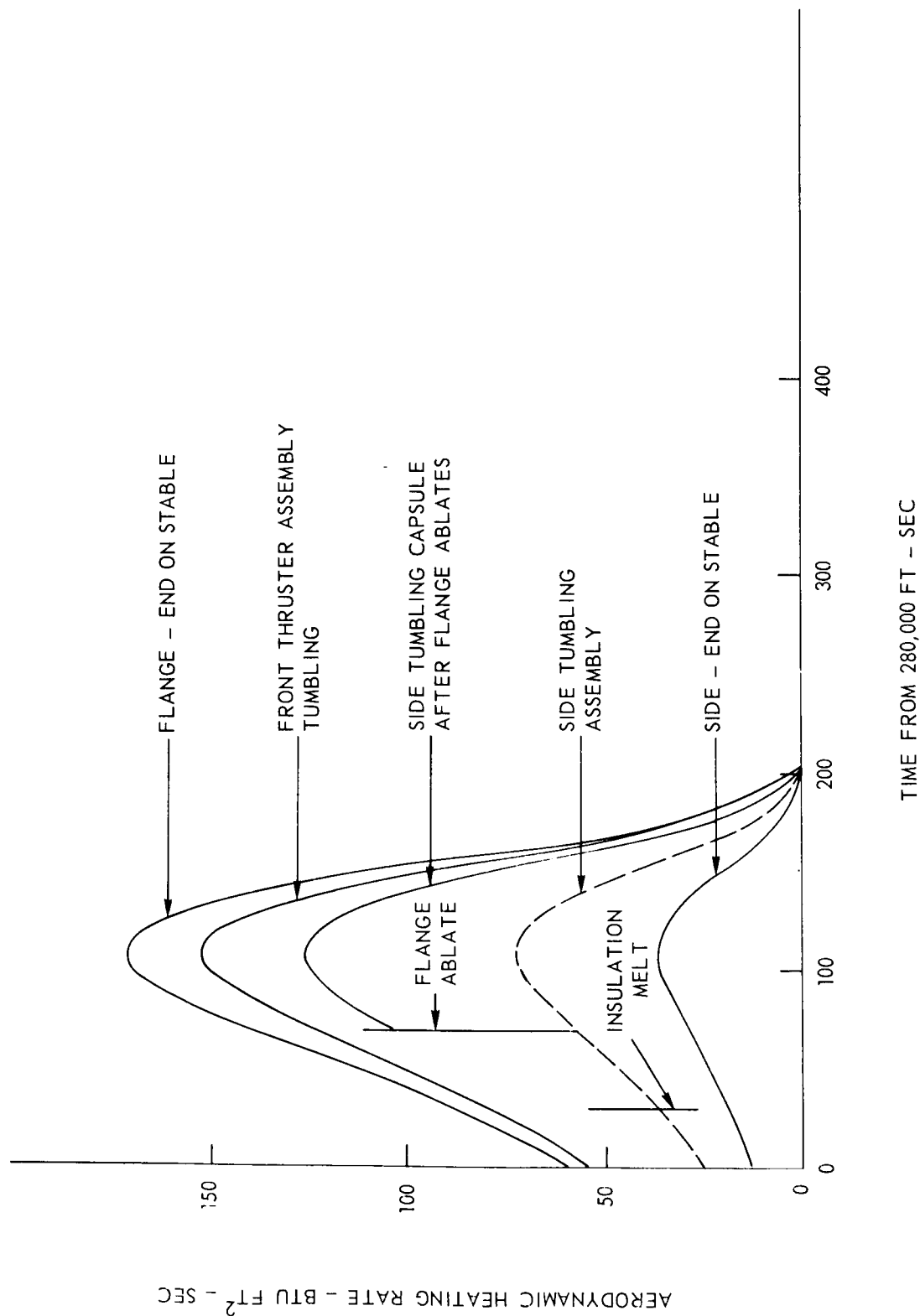
Figure 9. Radioisojet Assembly Released At 280,000 ft From Spacecraft Parking Orbit Decay Trajectory Aerodynamic Heating

26
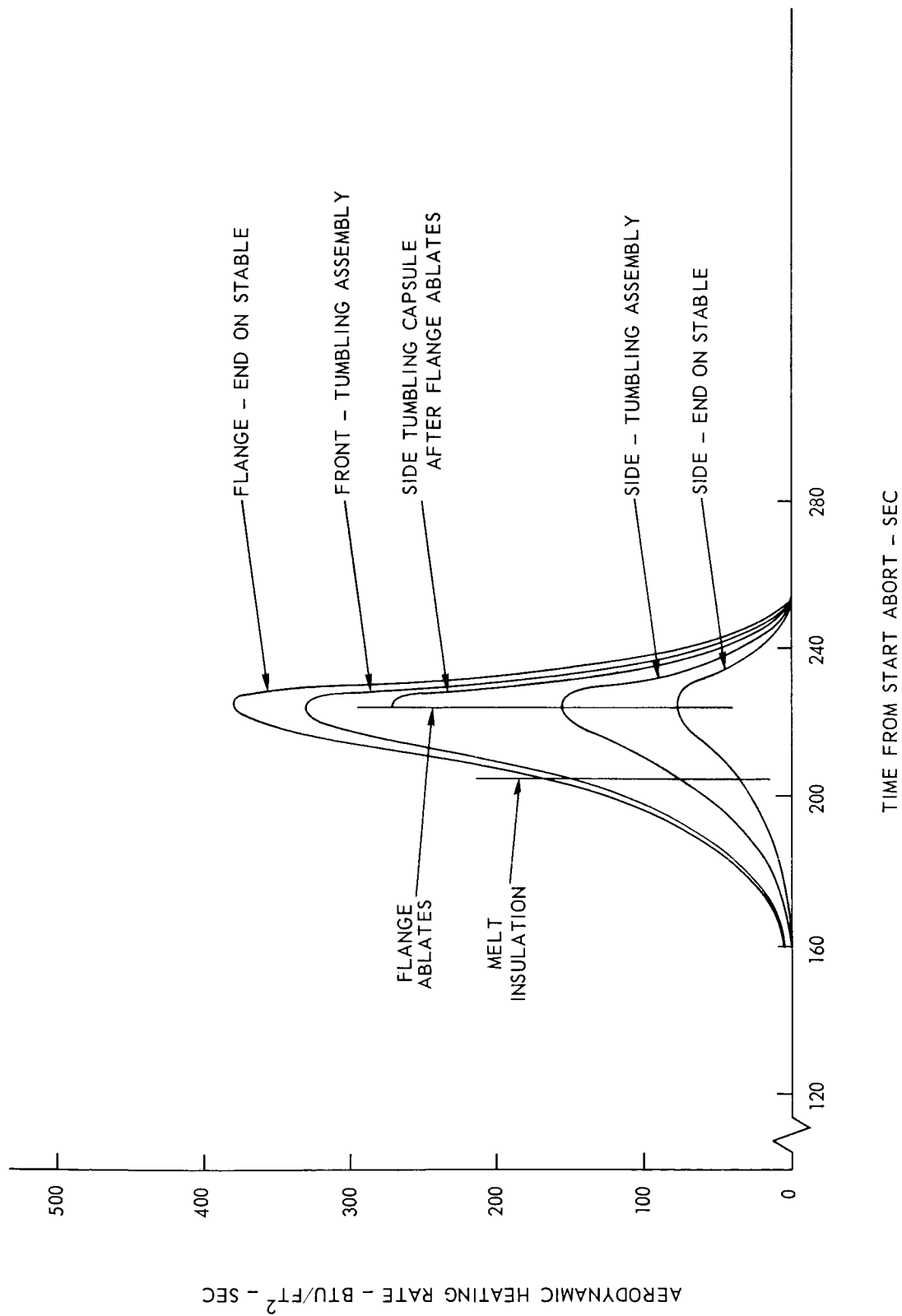
Figure 10. Radioisojet Thruster Released At EVM Abort Aerodynamic Heating

27
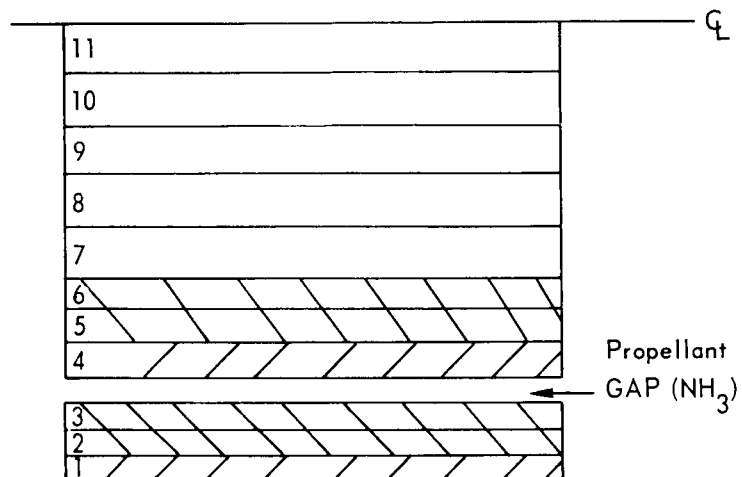
NODE 12 – Space

Stainless Steel	Node 1
Hastelloy X	Nodes 2, 3, 4
Refractory liner	Nodes 5, 6
Fuel (Pm_2O_3)	Nodes 7-11

Figure 11. Radioisojet Thermal Model
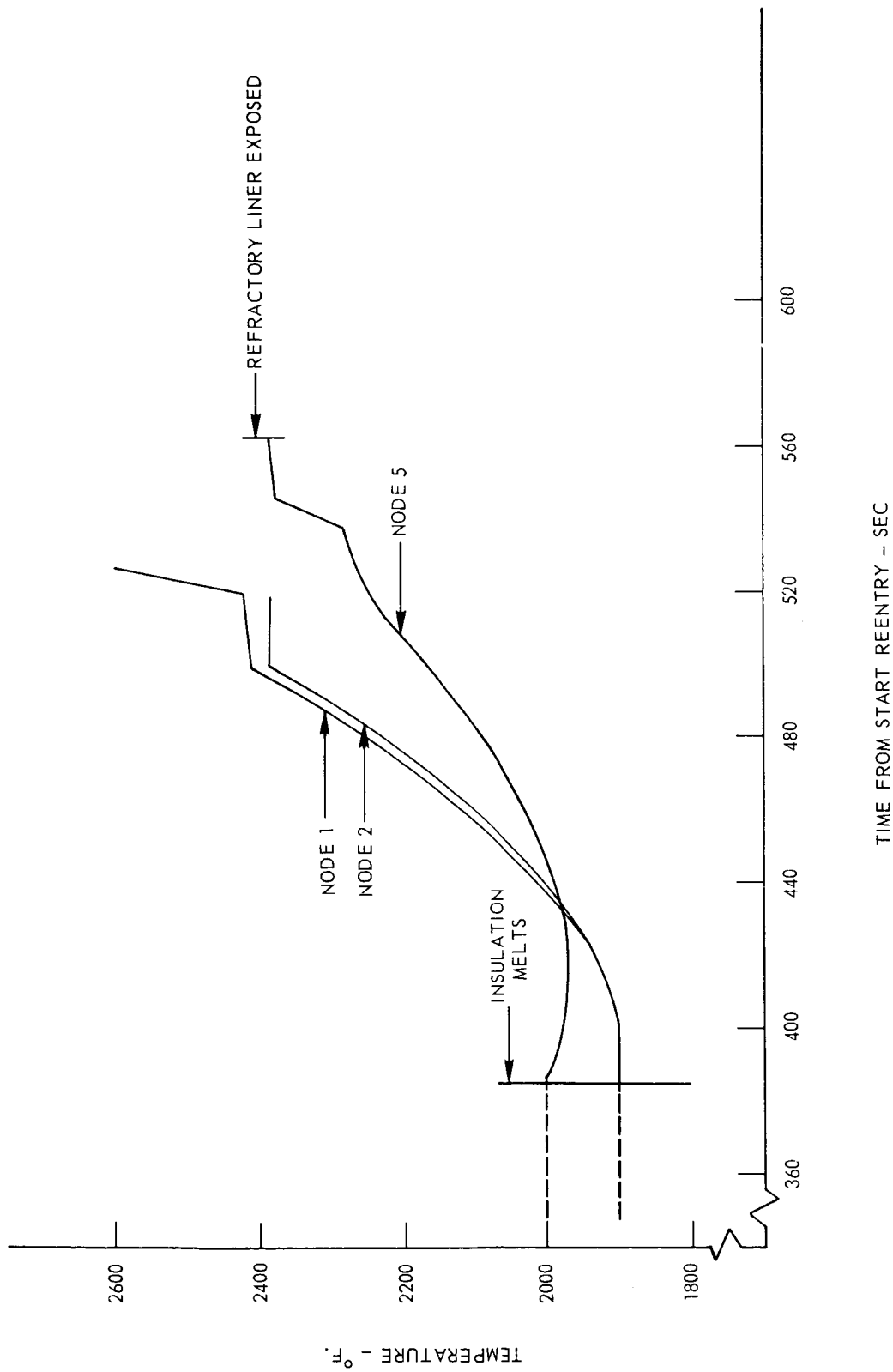
Figure 12. Radioisojet Temperature History During Reentry Parking Orbit Decay Trajectory Attached To Tumbling Spacecraft
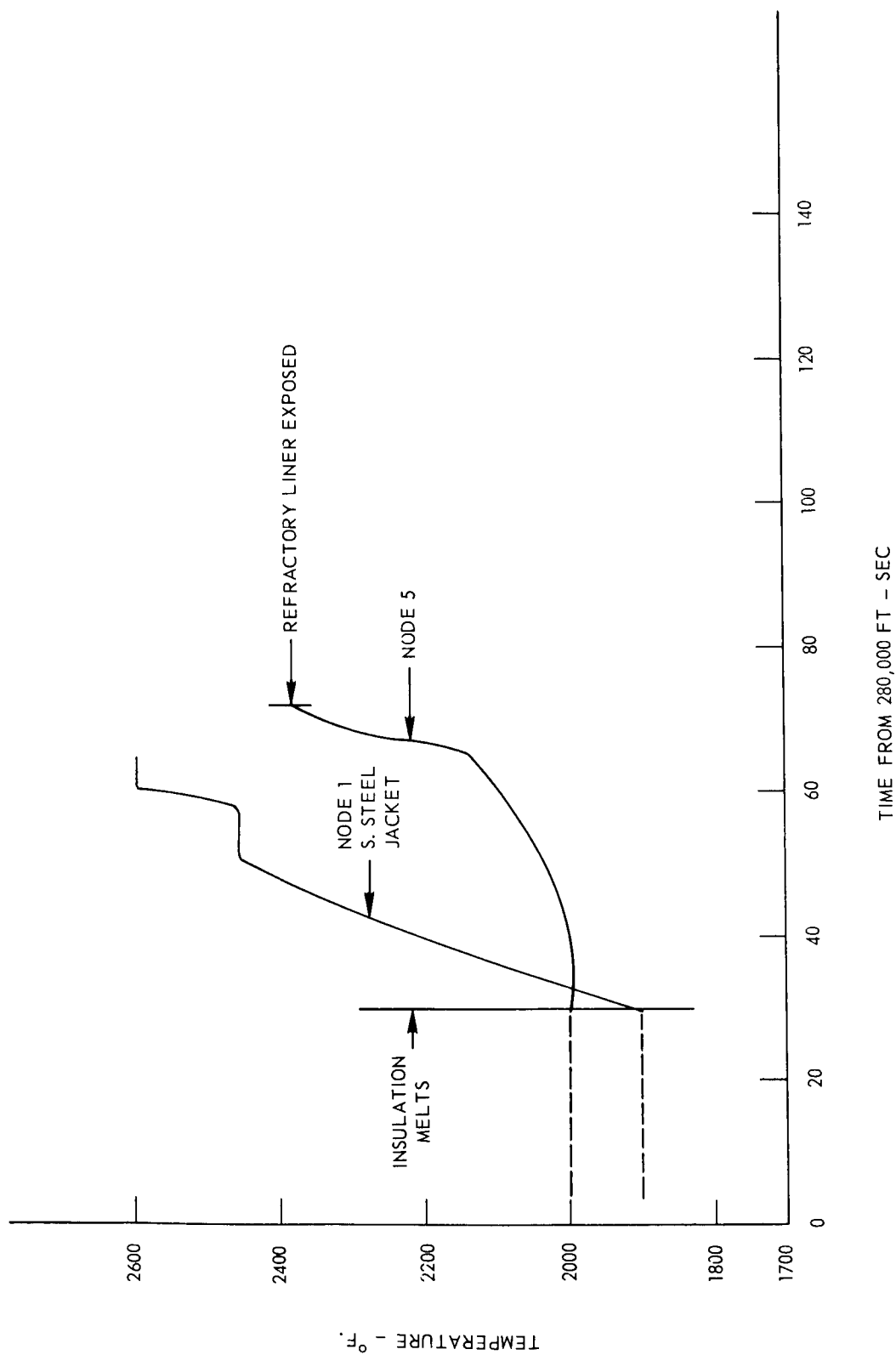
Figure 13. Radioisojet Temperature History During Reentry Parking Orbit Decay Trajectory Thruster Released At 280,000 ft
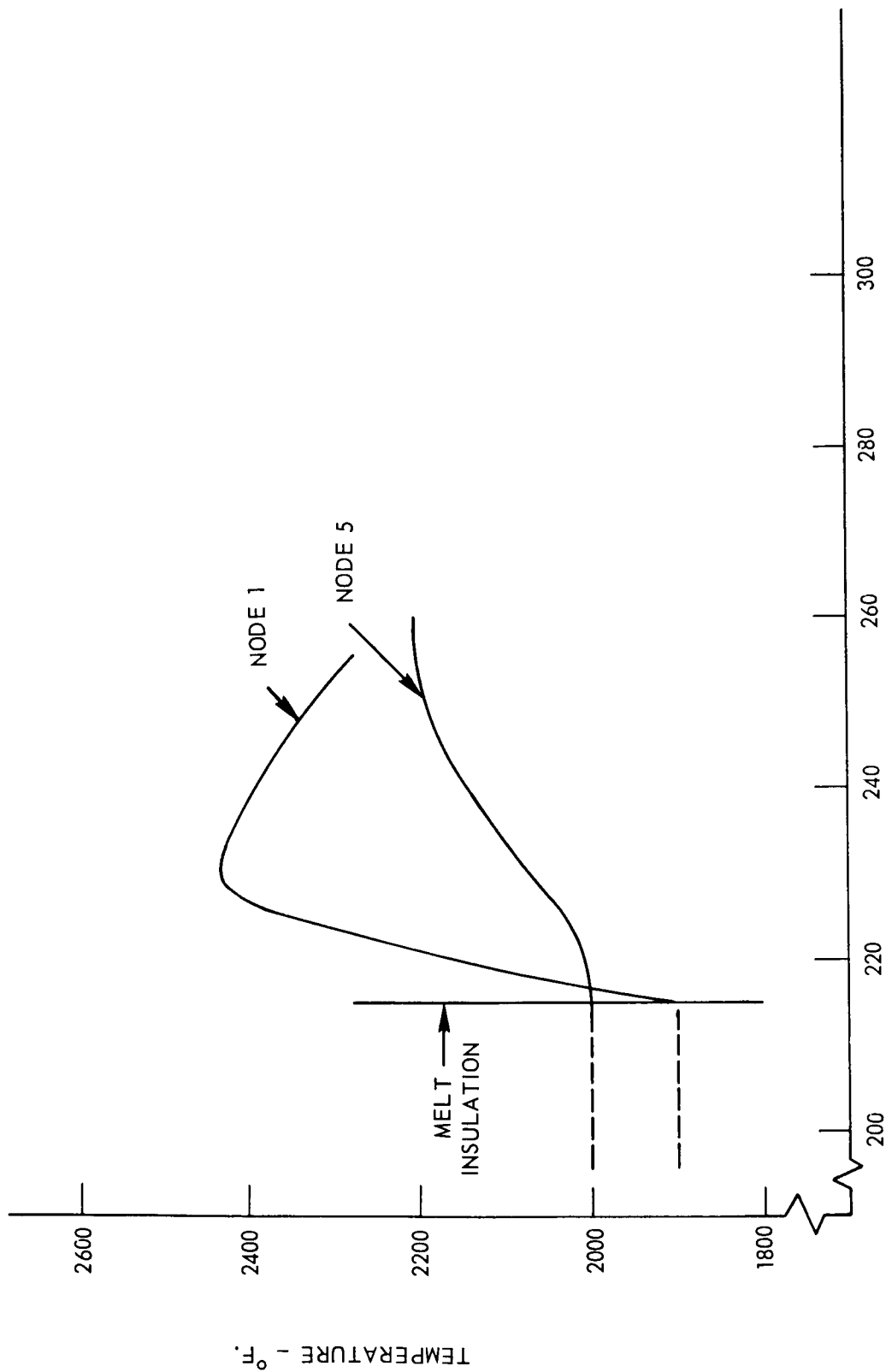
30
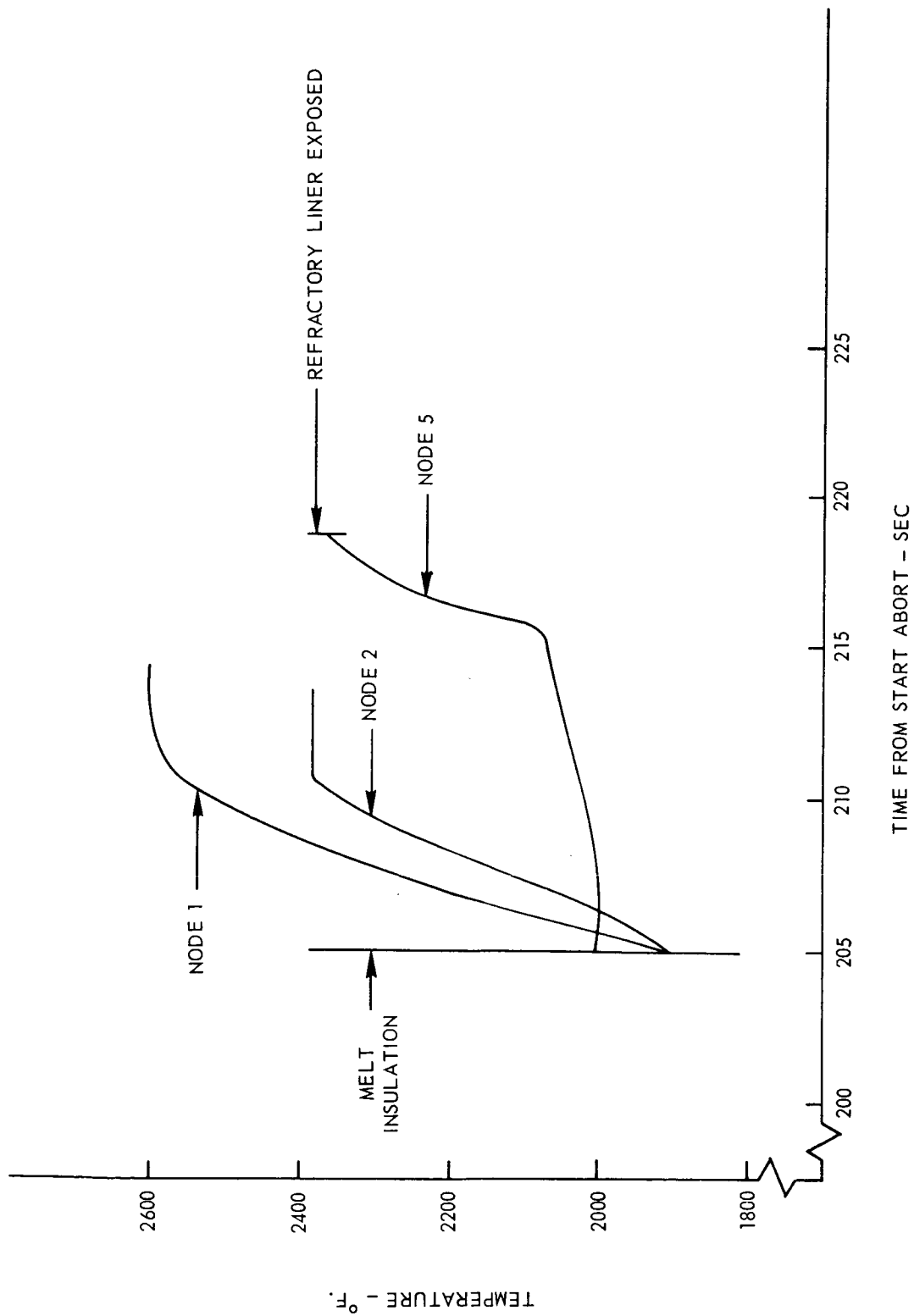
Figure 14. Radioisojet Temperature History During Reentry Thruster Released At EVM Abort.

31

Figure 15. Radioisojet Attached To Tumbling Spacecraft Booster Abort At EVM

32

① INTACT THRUSTER

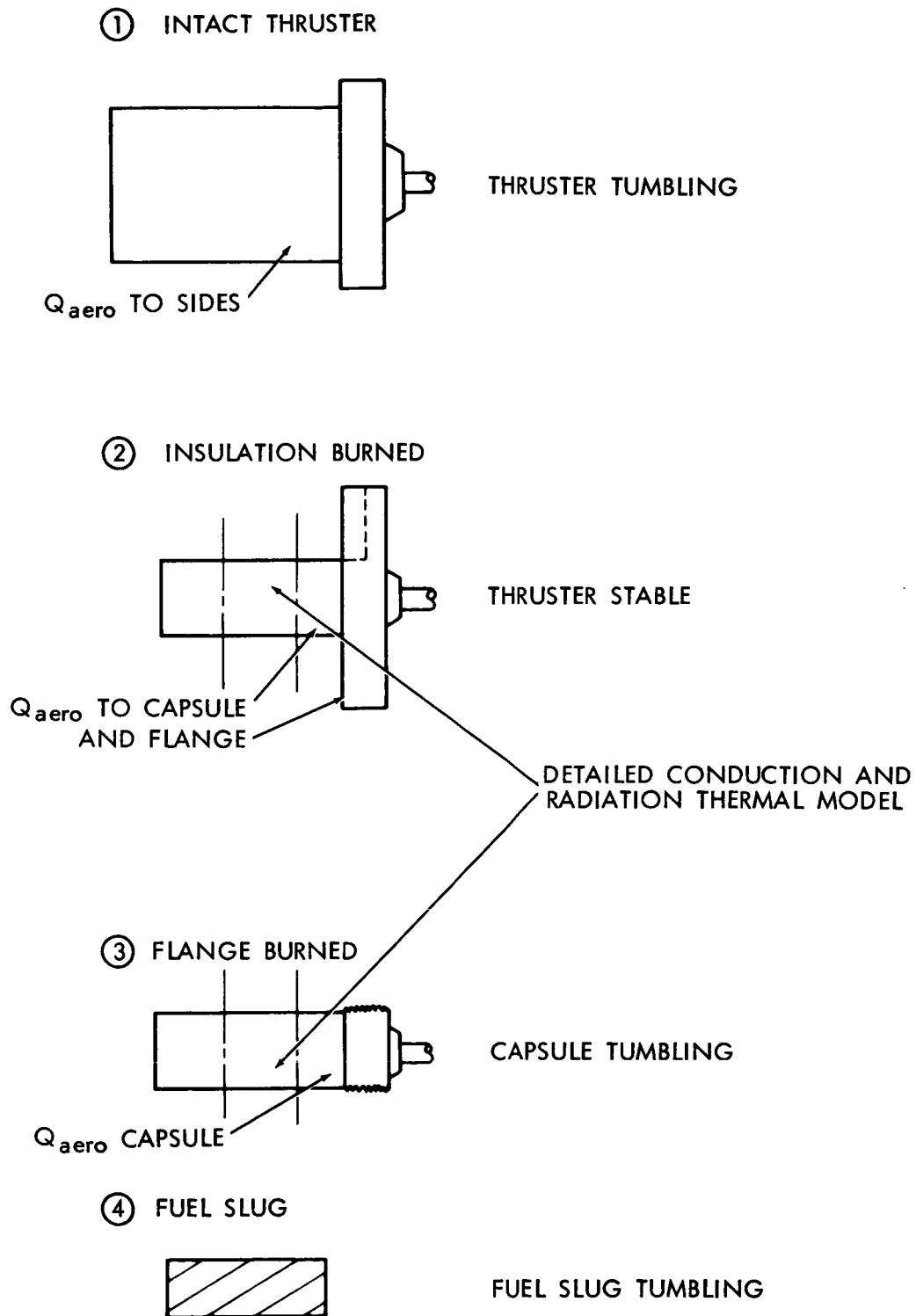THRUSTER TUMBLING

Q_{aero} TO SIDES

② INSULATION BURNED

THRUSTER STABLE

Q_{aero} TO CAPSULE
AND FLANGE

DETAILED CONDUCTION AND
RADIATION THERMAL MODEL

③ FLANGE BURNED

CAPSULE TUMBLING

Q_{aero} CAPSULE

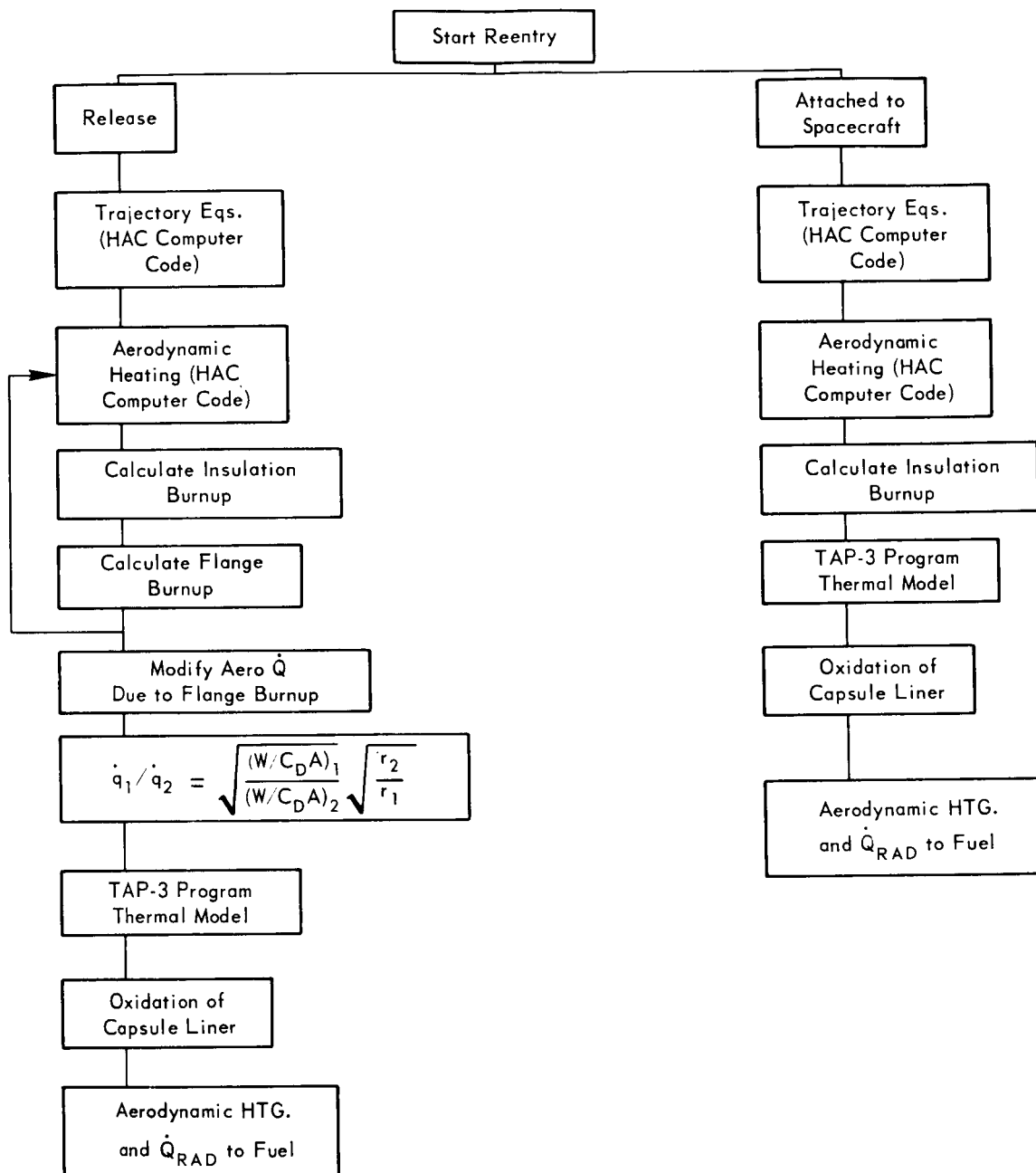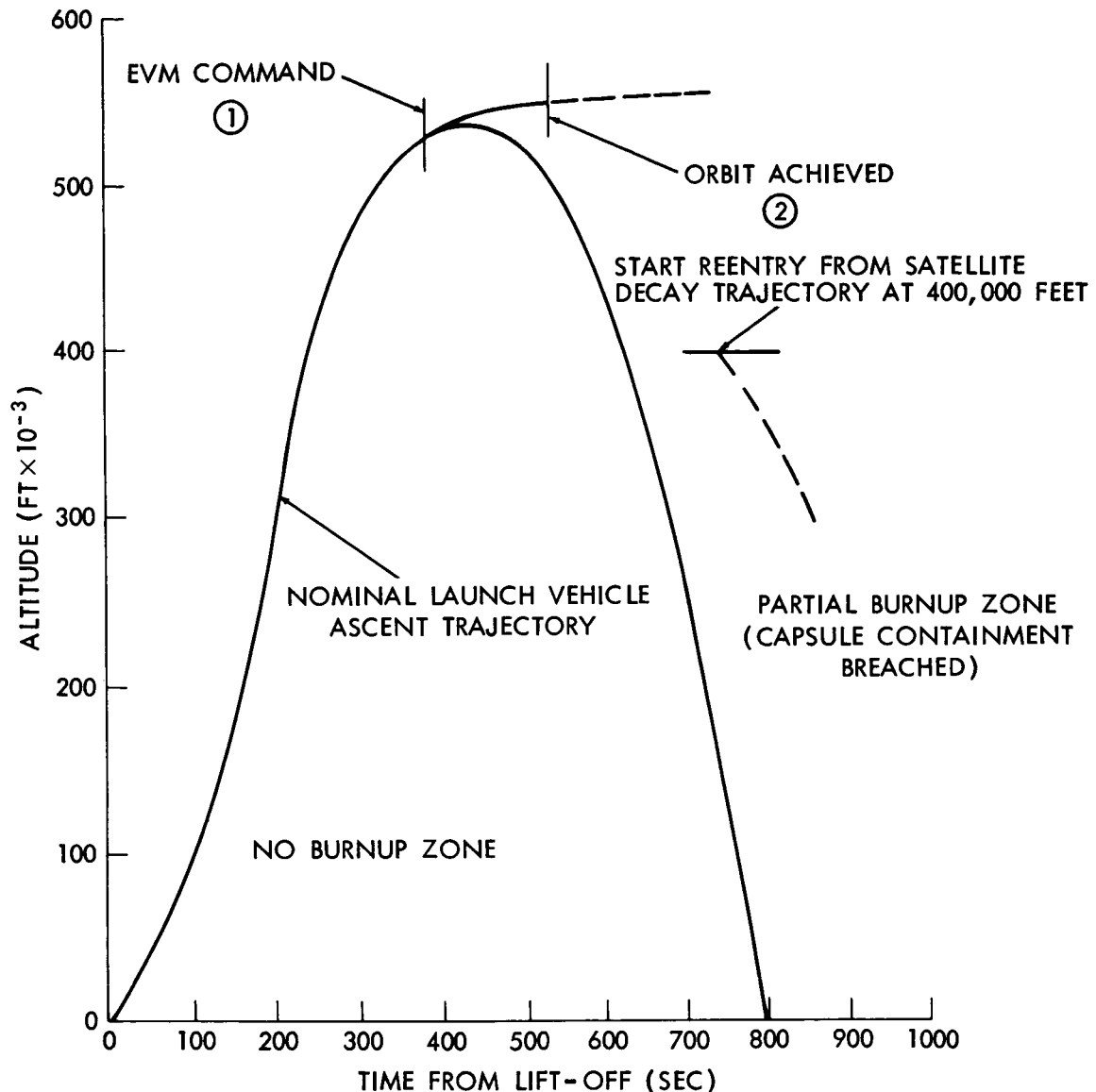④ FUEL SLUG

FUEL SLUG TUMBLING

Figure 16. RIJ Burnup Sequence Thruster Released

NOTES:

1. HAC: Hittman Aero Code – reentry trajectory and aerodynamic
   heating computer program

2. TAP-3: Thermal Analyzer Program – heat transfer and ablation
   computer program

Figure 17. Flow Diagram of Radioisojet Burnup Analysis

(1) Aborts occurring between Launch Vehicle lift-off and point ① result in the fuel capsule containment reentering intact; i.e., no Burnup for either the RIJ attached to the S/C or released from the S/C at the abort point.

(2) All aborts occurring between points ① and ② on the ascent trajectory result in breaching the fuel capsule containment upon reentry.

(3) S/C orbit is achieved after point ②. Eventual reentry from all satellite decay trajectories for the RIJ either attached to or released from the S/C result in breaching the fuel capsule containment. All satellite orbits are assumed to decay to an altitude of 400,000 feet prior to beginning atmospheric reentry trajectory.

(4) All data presented is based on initial postulated RIJ modes of release.
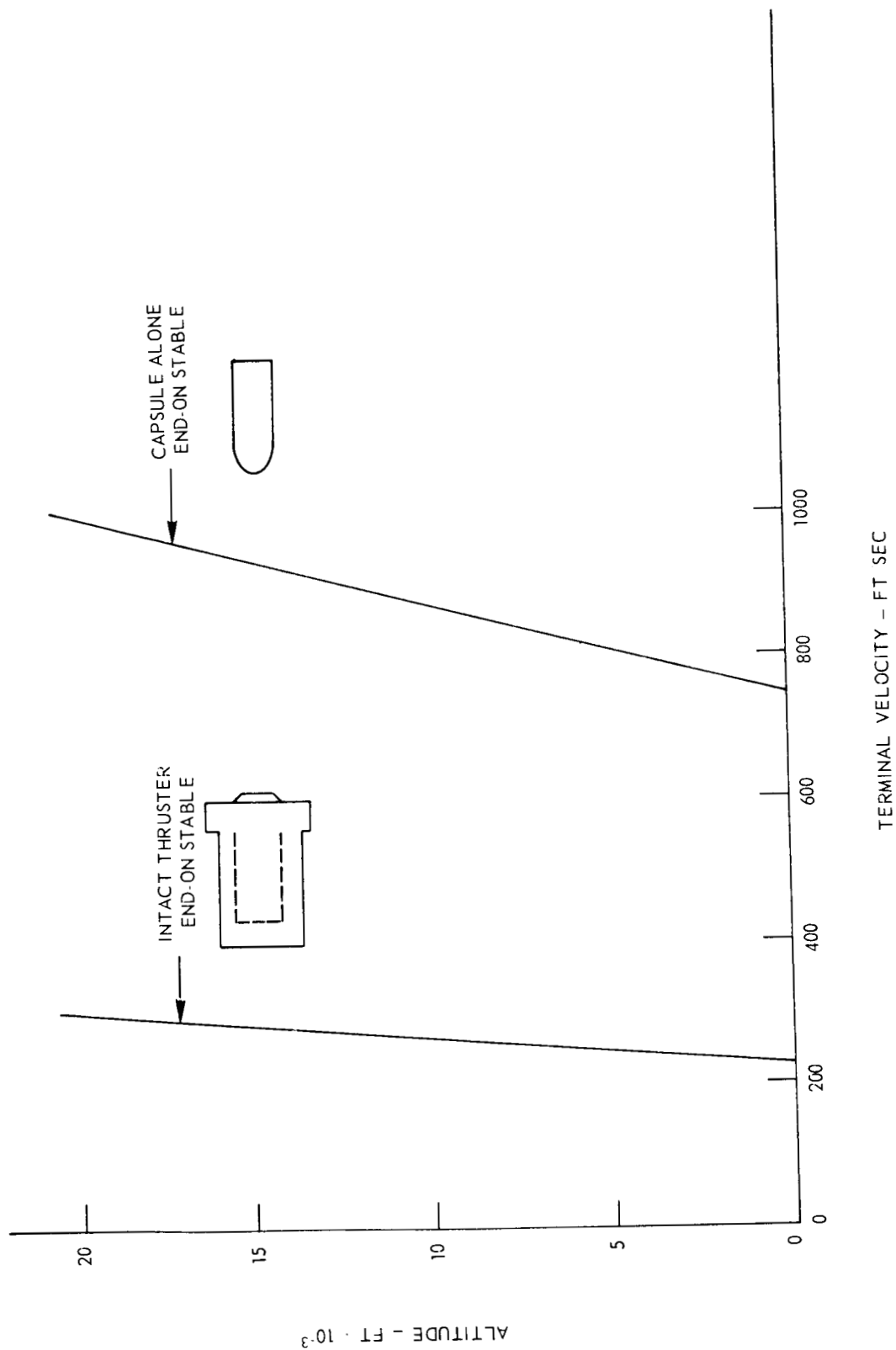
Figure 18. Radioisojet Burnup Zones

Figure 19. Radioisojet Terminal Velocity vs Altitude